Journal of Renewable Materials

Tech Science Press

DOI: 10.32604/jrm.2021.015824

ARTICLE

An α-Fe_2O_3/Circulating Fluidized Bed Fly Ash Based Geopolymer Composite Anode for Electrocatalytic Degradation of Indigo Carmine Dye Wastewater

Jiaqian Lei, Yaojun Zhang* and Panyang He

College of Materials Science and Engineering, Xi'an University of Architecture and Technology, Xi'an, 710055, China

*Corresponding Author: Yaojun Zhang. Email: zhangyaojun@xauat.edu.cn

Received: 16 January 2021 Accepted: 15 March 2021

ABSTRACT

Geopolymers have been developed to various catalysts due to their advantages. However, low conductivity restricts their application in the electrocatalysis field. In this study, an α-Fe_2O_3/circulating fluidized bed fly ash based geopolymer (CFAG) composite anode was fabricated using a facile dip-coating method by loading α-Fe_2O_3 in the matrix of CFAG. The effects of α-Fe_2O_3 content on the composition, surface morphology and electrochemical performance of α-Fe_2O_3/CFAG composite anode were investigated. The X-ray diffraction (XRD) and scanning electron microscope (SEM) results demonstrated that α-Fe_2O_3 was successfully inlaid with the surface of amorphous CFAG matrix. The electrochemical measurements indicated that α-Fe_2O_3/CFAG composite anode had higher oxygen evolution potential, greater electrochemical activity area, and smaller electrochemical impedance than CFAG. The as-prepared composite anode was applied for electrocatalytic degradation of indigo carmine dye wastewater. It was discovered that the highest degradation efficiency over 10α-Fe_2O_3/CFAG reached up 92.6%, and the degradation of indigo carmine followed pseudo-first-order kinetics. Furthermore, 10α-Fe_2O_3/CFAG composite anode presented excellent stability after five cycles. The active hydroxyl radical was generated over the α-Fe_2O_3/CFAG composite anode, which acted as strong oxidizing agents in the electrocatalytic degradation process.

KEYWORDS

Geopolymers; composite anode; electrocatalytic oxidation; dye degradation

1 Introduction

In recent years, with the rapid development of textile industry, the discharge of dye wastewater is increasing, which causes various harmful impacts on organisms and the environment. The complex composition, high organics, poor bio-degradability, high chromaticity and toxicity of the dye wastewater render it one of the most difficult industrial wastewater to treat [1,2]. In the textile industry, indigo carmine is one of the most popular dyes naturally, mainly for coloring of denim goods. An average of 3–12 g of indigo carmine is needed to color a pair of blue jeans. Therefore, the textile dyeing and washing industries are one of the major sources of indigo carmine dye emissions into the environment [3]. It has been a long-term challenge to effectively treat dye wastewater. Traditional physical, chemical and biological methods for treatment of dye wastewater still have disadvantages of high cost, low efficiency, extra pollution and complicated process procedures [4]. Therefore, it is urgent to develop a

novel treatment process with high efficiency and low energy for dye wastewater. At present, advanced oxidation processes (AOPs) have been considered to be a promising method for wastewater treatment, mainly including photocatalysis, catalytic ozonation, wet air oxidation, electrochemical advanced oxidation process (EAOPs), and Fenton or Fenton-like reaction, etc. [5,6]. Among these methods, EAOPs have attracted more attention because of its high efficiency, easy operation, mild reaction conditions, less pollution, and small occupation [7]. Anode material is core component in EAOPs for its high oxidation performance, which is caused by direct electron transfer on the anode surface and indirect oxidation of strongly oxidizing free radicals [8]. An ideal anode should have characteristics of high catalytic activity, high stability, high oxygen evolution potential, long service lifetime and low cost [9]. Up to now, the anode materials have been investigated mainly including Pt, graphite, dimensionally stable anodes (DSA) and boron-doped diamond (BDD). de Oliveira et al. [10] reported that the electrocatalytic degradation of methylene blue dye by Pt anode had good decolorization removal under different conditions. Alcocer et al. [11] compared the degradation of various dyes by the EAOPs, electro-Fenton, photoelectro-Fenton process using BDD electrode, and the EAOPs/BDD process had great potential for degradation of dye wastewaters. However, both Pt and BDD have an obvious problem of high cost, so they are not suitable for industrialized application. Kong et al. [12] reported that graphite as an anode material had good electrocatalytic degradation of methyl orange and could be considered as an excellent material for the treatment of dye wastewater. The graphite anodes are economical but their oxygen evolution potential is low. As typical DSA, Ti/PbO_2 and Ti/SnO_2 anode have been illustrated to be excellent materials for electrocatalytic degradation of dye wastewater. The PbO_2 anode has strong conductivity, good mechanical properties and high oxygen evolution potential, but it is limited in practical application due to its poor catalyst activity and easy exfoliation [13]. SnO_2 anode shows high oxygen evolution potential, easy preparation and low cost, but it suffers from poor stability and short service life [14]. Therefore, the scholars have studied many ways to improve the above problems, including adjusting substrate, building interlayer and modifying oxide coatings [13]. Wu et al. [15] fabricated a novel anode with TiO_2 nanotube array as a tubal template and the Sb-SnO_2 coating as an interlayer, which significantly enhanced electrocatalytic activity and lifetime of PbO_2 anode. Xu et al. [16] modified the Ti/SnO_2-Sb interlayers with copper nanotubes to improve the conductivity and service life of SnO_2 anode. Based on the aforementioned backgrounds, it is necessary to develop novel composite anodes with low cost and high efficiency for electrocatalytic degradation of dye wastewater.

Geopolymer (GP) is fabricated by reacting alkali-activator solutions with industrial solid wastes, such as fly ash, coal gangue, slag, and various tailings. Geopolymer, a type of aluminosilicate material with unique three-dimensional network structure, has been widely used in the fields of building materials, environmental protection and chemical industry due to its excellent mechanical, durability, adsorption and catalysis properties [17]. As a new type of catalyst, GP are easier to obtain and cheaper than other catalysts reported [18]. Zhang et al. [19] used fly ash based geopolymer as a photocatalyst for the degradation of dye wastewater. However, the low conductivity limited their applications in the electrocatalysis field. Transition metal oxides, especially α-Fe_2O_3 have attracted more attention because of their high activity and better stability [20]. Choi et al. [21] discussed the effect of the addition of Fe_2O_3 on the physical property of geopolymer. Chen et al. [22] synthesized Fe_2O_3-modified porous geopolymer microspheres composites by *in-situ* co-precipitation process for the adsorptive removal and solidification of F^- from wastewater. Therefore, we predict that composite anode synthesized by loading α-Fe_2O_3 in the matrix of GP is promising to improve the electrochemical properties and the stability of the inherent anode.

In this study, a novel α-Fe_2O_3/circulating fluidized bed fly ash based geopolymer (CFAG) composite anode is prepared using the dip-coating method by combining α-Fe_2O_3 with alkali-activated CFAG onto stainless steel substrate. The utilization of CFAG as matrix for preparation of composite anode can not only realize the recycle utilization of industrial solid wastes, but also enrich the types of electrocatalytic

anode materials. Moreover, the composite anode is used for electrocatalytic degradation of dye wastewater, which is of great significance to the wastewater treatment of textile industry. And to the best of our knowledge, there are not any reports about the preparation and electrochemical performance of the α-Fe_2O_3/CFAG composite anodes.

2 Materials and Methods

2.1 Materials

Circulating fluidized bed fly ash (CFBFA) was provided by Shenhua Junggar Energy Co., Ltd. The main chemical compositions of CFBFA were measured by the mass percent using X-ray fluorescence (XRF), as shown in Tab. 1. α-Fe_2O_3 with the size of 30 nm was purchased from Shanghai McLean Biochemical Technology Co. Ltd., KOH (AR), NaOH (AR), Na_2SiO_3 (AR), oxalic acid, ethanol, and tertiary butyl alcohol were obtained from the Tianjin Yaohua Chemical Reagent Co. Ltd., Stainless steel (SS) sheets of size 20 mm × 15 mm × 0.2 mm were purchased from Shanghai Huapeng Metal Co., Ltd., Shanghai. The water is deionized water.

Table 1: Chemical compositions of CFBFA

SiO_2	Al_2O_3	Fe_2O_3	CaO	P_2O_5	MgO	Na_2O	K_2O	SO_3	TiO_2	LOSS
36.33	44.47	1.93	2.82	0.20	0.26	0.09	0.40	0.55	1.92	11.03

2.2 Preparation of α-Fe_2O_3 /CFAG Composite Anode

The SS sheet as anode substrate was polished with abrasive paper and then degreased in the 40 wt% NaOH aqueous solution several times. The treated SS sheet was etched in 10 wt% oxalic acid to remove the surface oxide layer. Then, the SS sheet was rinsed with deionized water and dried at 80°C. The synthesis steps of α-Fe_2O_3/CFAG composite anode was described as follows: the composite slurry was prepared by mixed CFBFA, α-Fe_2O_3, KOH, Na_2SiO_3, and water at the mass ratio of 1:0.03:0.028:0.37:0.5. The slurry was cured at 80°C for 8 h in the oven to obtain the α-Fe_2O_3/CFAG composite. For the preparation of the composite anode, the slurry was dip-coated onto the pretreated SS substrate (effective coating area 15 mm × 15 mm × 0.2 mm), and the α-Fe_2O_3/CFAG composite anode was obtained after curing at same condition. The sample added 3wt% α-Fe_2O_3 was marked as 3α-Fe_2O_3/CFAG. Similarly, the samples containing 10wt% α-Fe_2O_3 and 20wt% α-Fe_2O_3 were separately obtained and named as 10α-Fe_2O_3/CFAG and 20α-Fe_2O_3/CFAG. The sample without α-Fe_2O_3 was denoted as CFAG. The main chemical compositions of different anode materials were shown in Tab. 2.

Table 2: Chemical compositions of samples

Sample	SiO_2	Al_2O_3	Fe_2O_3	CaO	P_2O_5	MgO	Na_2O	K_2O	SO_3	Ti_2O
CFAG	38.02	32.98	1.76	1.68	0.09	0.18	8.48	2.68	0.27	1.71
3α-Fe_2O_3/CFAG	37.23	31.79	3.92	1.59	0.09	0.18	8.83	2.64	0.26	1.70
10α-Fe_2O_3/CFAG	35.57	31.98	7.51	1.58	0.08	0.17	8.21	2.64	0.25	1.70
20α-Fe_2O_3/CFAG	34.89	31.73	12.8	1.47	0.08	0.17	7.78	2.60	0.20	1.68

2.3 Characterization of α-Fe_2O_3 /CFAG Composite Anode

The chemical compositions of the various samples were characterized in the elemental range of Be4~U92 using a S4 P10NEER X-ray fluorescence (XRF) spectrometer worked at 60 kV and 150 mA. The X-ray diffraction (XRD) patterns were obtained on a Rigaku D/Max 2200 diffractometer in the 2θ

range of 5~70° with a speed of 10°/min under operating at 40 mA and 40 kV. The microstructure was investigated on a FEI Quanta 200 scanning electron microscope (SEM) equipped with energy-dispersive X-ray spectroscopy (EDS). The X-ray photoelectron spectroscopy (XPS) were recorded on an AXIS SUPRA analyzer using monochromatic Al Kα anode target operated at 15 kV and 8 mA. All electrochemical measurements were analyzed by a CHI660E electrochemical workstation with the three-electrode system. Platinum plate (Pt), saturated calomel electrode (SCE) and as-prepared anode were used as counter electrode, reference electrode and working electrode, respectively.

2.4 Electrocatalytic Degradation of Dye Wastewater

The electrocatalytic properties of composite anodes were evaluated by simulated degradation of dye wastewater of indigo carmine. The as-prepared electrode as an anode, and SS sheet with the same surface area as a cathode, were used for the electrocatalytic degradation of 50 mL indigo carmine dye wastewater (15 mg/L) containing 0.1 M Na_2SO_4 electrolyte under magnetic stirring. Meanwhile, the external bias was 0.8 V, and the space between cathode and anode was 2 cm. The initial absorbance (A_0) of indigo carmine dye (the corresponding concentration (C_0)) was analyzed by UV-Vis spectrophotometer at maximum absorption wavelength of 610 nm. The absorbance (A_t) at 10 min intervals (the corresponding concentration (C_t)) was measured from the supernatant solution by centrifugal separation method. The degradation rate (DR) was calculated by the equation as follows:

$$DR(\%) = (C_0 - C_t)/C_0 \times 100\% = (A_0 - A_t)/A_0 \times 100\% \quad (1)$$

3 Results and Discussion

3.1 Microstructure of as-Prepared Composite Anodes

Fig. 1a shows XRD patterns of various anode materials. The pattern for α-Fe_2O_3 there appears the diffraction peaks at 2θ of 24.2°, 33.2°, 35.7°, 40.9°, 49.4°, 54.1°, 62.4°, and 64.1° corresponding to (012), (104), (110), (113), (024), (116), (018) and (214) crystal planes of α-Fe_2O_3 (JCPDS 33-0664), respectively. The pattern for CFAG displays a broad diffuse hump in the range of 20° to 40°, indicating the formation of amorphous geopolymer gels [23]. It is difficult to observe the characteristic peaks of α-Fe_2O_3 phase in 3α-Fe_2O_3/CFAG composite anode, which may be due to the low loading and amorphous distribution of α-Fe_2O_3 on the surface of CFAG matrix. There are three new peaks of 10α-Fe_2O_3/CFAG and 20α-Fe_2O_3/CFAG appeared in the characteristic peaks of α-Fe_2O_3 phase at 2θ = 33.2°, 35.7°, and 54.1°. The peak intensities have a slight increase with increasing loading. In addition, the remaining mineral phases of 10α-Fe_2O_3/CFAG and 20α-Fe_2O_3/CFAG have not changed, indicating that CFAG as matrix has good stability. The surface compositions of the composite anode are analyzed by XPS. The full spectrum of 10α-Fe_2O_3/CFAG specimen in Fig. 1b is mainly made up of Si, Al, Na, O, C, and Fe. Fig. 1c shows the high-resolution XPS spectra of Fe 2p. Fe 2p spectrum exhibits two main peaks at 711.1 eV (Fe $2p_{3/2}$) and 724.3 eV (Fe $2p_{1/2}$), respectively, which match well with the characteristic peak of Fe^{3+} [24]. It confirms the existence of Fe^{3+} in the form of α-Fe_2O_3 in the as-synthesized composite anode.

Fig. 2a shows SEM image of CFAG anode surface, indicating that CFBFA dissolved and condensed forming the geopolymer binder. The uniform surface of CFAG anode provides favorable conditions for the loading of α-Fe_2O_3. SEM images of the composite anode surface loading different α-Fe_2O_3 are shown in Figs. 2b–2d. As can be seen, the surface of 3α-Fe_2O_3/CFAG and 10α-Fe_2O_3/CFAG is more homogeneous, dense, and without obvious cracks, which can greatly increase the effective active area, improve the chemical corrosion resistance and stability, and extend anode life [25]. However, the rough and porous surface of 20α-Fe_2O_3/CFAG may be due to the aggregation of α-Fe_2O_3, which will reduce the

bonding force between the SS substrate and the coating, resulting in the coating to fall off and reduction in catalytic activity. It can be seen that appropriate α-Fe_2O_3 loading can significantly improve the microstructure of the anode surface and enhance the electrocatalytic activity. As shown in Fig. 2e, the thickness of 10α-Fe_2O_3/CFAG composite anode coating is about 100 μm. Moreover, EDS spectrums are further used to verify the elemental composition of the anode materials. The results (Figs. 2f–2i) indicate that the samples consist of Si, Al, Na, O, and Fe, and the mass ratio of Fe element increases with the increase of the α-Fe_2O_3 load. The results confirm that α-Fe_2O_3 has been inlaid with amorphous geopolymer surface. These are consistent with XRD results.

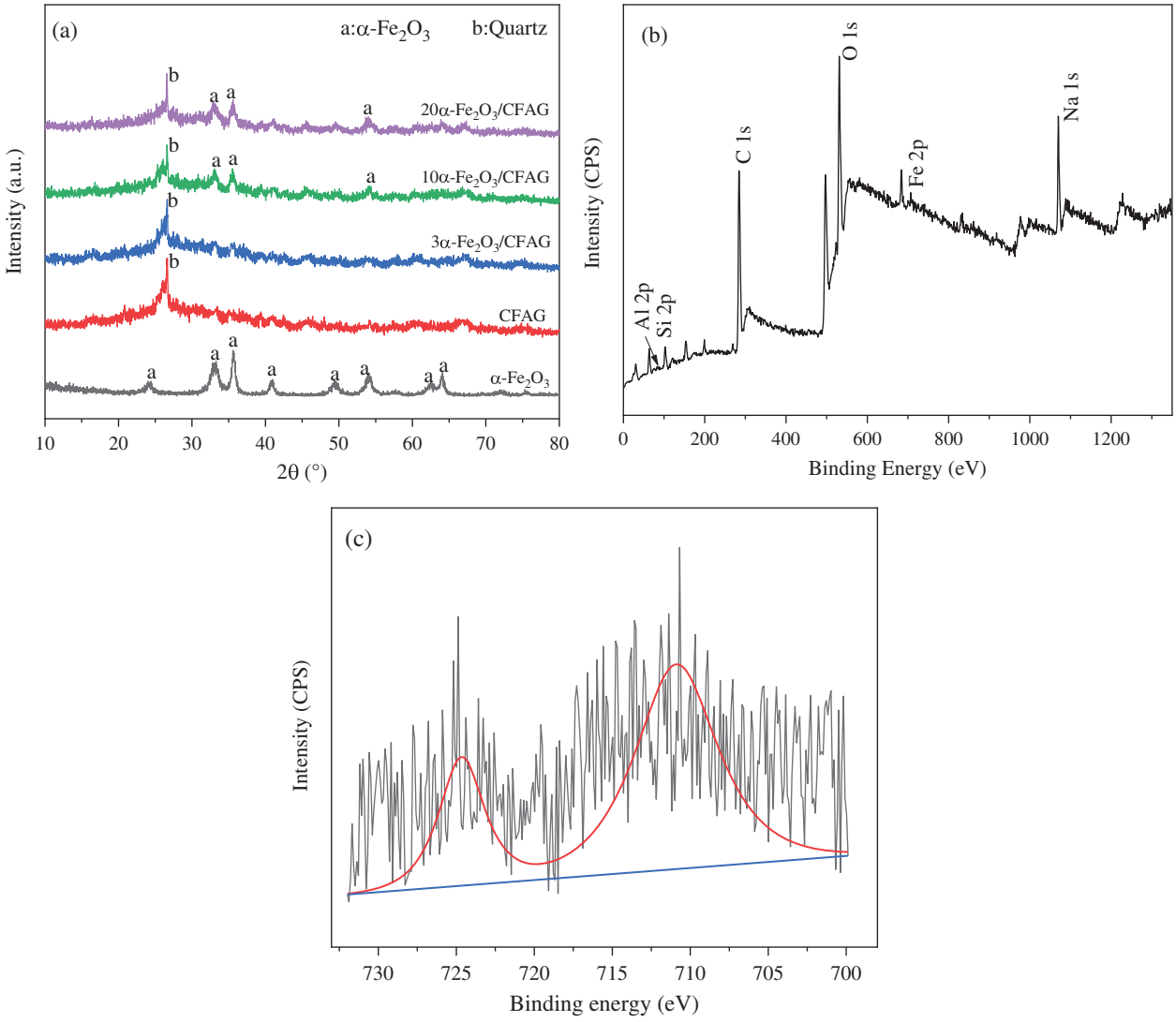

Figure 1: XRD patterns of (a) various specimens, XPS spectra of (b) 10α-Fe_2O_3/CFAG and (c) high resolution of Fe 2p

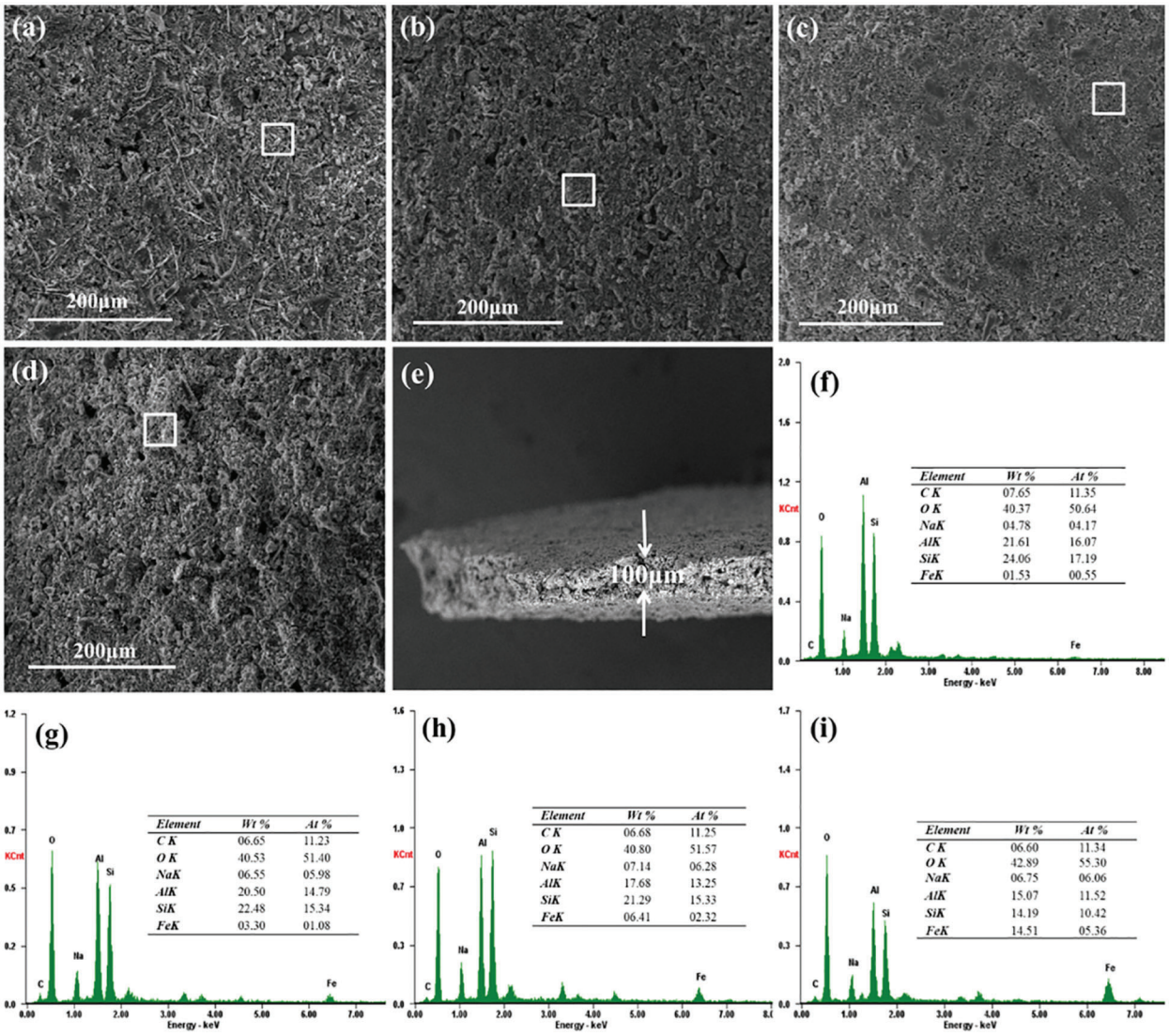

Figure 2: SEM images of (a) CFAG, (b) 3α-Fe_2O_3/CFAG, (c) 10α-Fe_2O_3/CFAG, and (d) 20α-Fe_2O_3/CFAG anode surface; (e) cross-section view of 10α-Fe_2O_3/CFAG coating; EDS results of (f) CFAG, (g) 3α-Fe_2O_3/CFAG, (h) 10α-Fe_2O_3/CFAG, and (i) 20α-Fe_2O_3/CFAG anode surface

3.2 Electrochemical Properties of as-Prepared Composite Anodes

Linear sweep voltammetry (LSV) curves are used to record the oxygen evolution of anode materials in the wastewater degradation process. As shown in Fig. 3a, LSV curves of the as-prepared anodes are obtained at scan rate of 100 mV/s in 0.5 M Na_2SO_4 supporting electrolyte. The oxygen evolution potentials (OEP) for CFAG, 3α-Fe_2O_3/CFAG, 10α-Fe_2O_3/CFAG, and 20α-Fe_2O_3/CFAG are measured to be 0.99 V, 1.20 V, 1.45 V, and 1.28 V (*vs*. SCE). Compared with CFAG anode, α-Fe_2O_3/CFAG composite anode has higher OEP, especially 10α-Fe_2O_3/CFAG. The oxygen evolution reaction easily occurs under a lower OEP, resulting in low current efficiency. Higher OEP can restrain the oxygen evolution side reaction to improve the electrocatalytic activity and reduce the energy consumption [26]. The cyclic voltammetry (CV) curves of as-prepared anodes are tested in 0.5 M Na_2SO_4 supporting solution at a scan rate of 100 mV/s, as shown in Fig. 3b. The result indicates that α-Fe_2O_3/CFAG composite anode has a higher

peak current density and a larger area of a curve than CFAG. The greater the current response is, the higher the electrochemical activity of the anode. Besides, a larger area of the CV curve is connected to more active sites on the anode surface [27]. The electron transfer performance of the as-prepared anodes are explored by electrochemical impedance spectroscopy (EIS) in 0.5 M Na_2SO_4 solution with the frequency range of 10^5-1 Hz. As shown in Fig. 3c, the Nyquist plot can be divided into a semicircle and inclined line, representing the electron transfer process and ion diffusion process, respectively. The semicircle diameter corresponds to the electron transfer resistance and the smaller the semicircle diameter is, the faster the rate of electron transfer rate as well as electrochemical reaction [28]. A relatively large semicircle is obtained on CFAG anode, demonstrating that it has a poor electron transfer process. With the increase of α-Fe_2O_3 loading, the semicircle diameter decreases gradually. The 10α-Fe_2O_3/CFAG composite anode has a smallest semicircle diameter, indicating that appropriate α-Fe_2O_3 can expose more electrochemical active sites to enhance the conductivity and decrease the interfacial resistance on the anode surface [13,29]. However, combined with the previous SEM analysis, the aggregation of α-Fe_2O_3 on the surface of 20α-Fe_2O_3/CFAG may cause a decrease of electrocatalytic activity. In summary, 10α-Fe_2O_3/CFAG composite anode with higher OEP, greater electrochemical activity area, and lower interfacial resistance is more suitable for electrocatalytic degradation of wastewater.

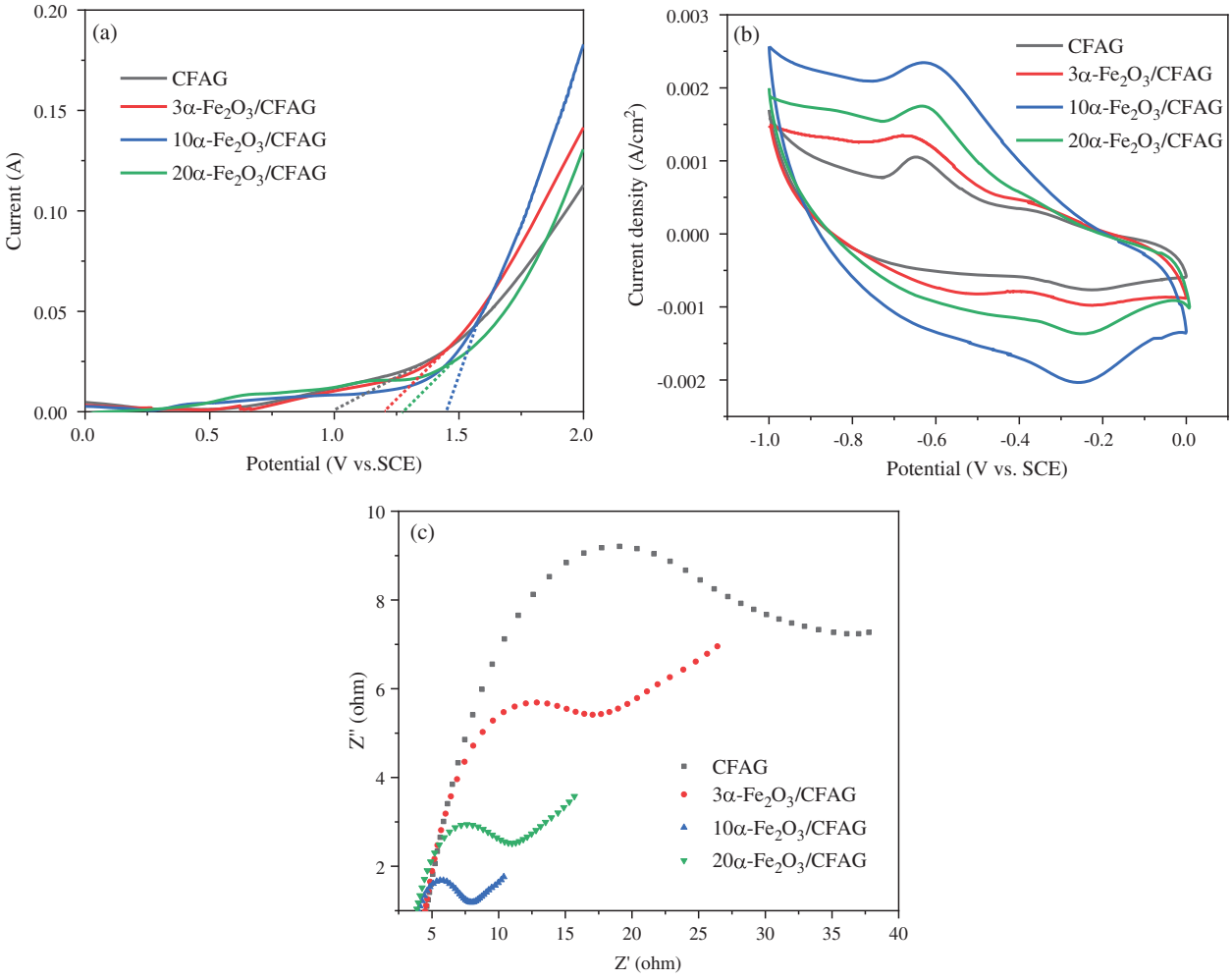

Figure 3: (a) LSV curves, (b) CV curves, (c) EIS Nyquist spectra of CFAG, 3α-Fe_2O_3/CFAG, 10α-Fe_2O_3/CFAG and 20α-Fe_2O_3/CFAG anodes in 0.5 M Na_2SO_4 solution

3.3 Degradation of Dye Wastewater

The as-prepared electrode as an anode, and SS sheet with the same surface area as a cathode, are used for the electrocatalytic degradation of indigo carmine dye wastewater. Fig. 4a displays the degradation of indigo carmine dye over different α-Fe_2O_3/CFAG anode materials. The degradation efficiency is in the sequence of 92.6% (10α-Fe_2O_3/CFAG) > 86.4% (20α-Fe_2O_3/CFAG) > 82.7% (3α-Fe_2O_3/CFAG) > 63.8% (CFAG). The result indicates that the performance of electrocatalytic degradation can be significantly improved by appropriate α-Fe_2O_3 loading. The 10α-Fe_2O_3/CFAG composite anode shows higher degradation efficiency than others, which is undoubtedly supported the electrochemical measurement results. Combined with the previous analysis, the degradation rate over 20α-Fe_2O_3/CFAG composite anode has decreased due to the reduction of electrocatalytic activity by aggregation of α-Fe_2O_3. The kinetics analysis is applied to further understand electrocatalytic degradation process of dye wastewater. Tab. 3 summarizes the kinetic parameters of pseudo zero-order, first-order, and second-order reactions for electrocatalytic degradation of indigo carmine over 10α-Fe_2O_3/CFAG composite anode. As shown in Fig. 4b, the decay of indigo carmine displays an exponential behavior, indicating that the degradation reaction accords with pseudo first-order kinetics. The value of kinetic rate constants (k = 0.03065) and correlation coefficient (R^2 = 0.979) reached the maximum over 10α-Fe_2O_3/CFAG, indicating that the optimum α-Fe_2O_3 loading is 10% for indigo carmine degradation.

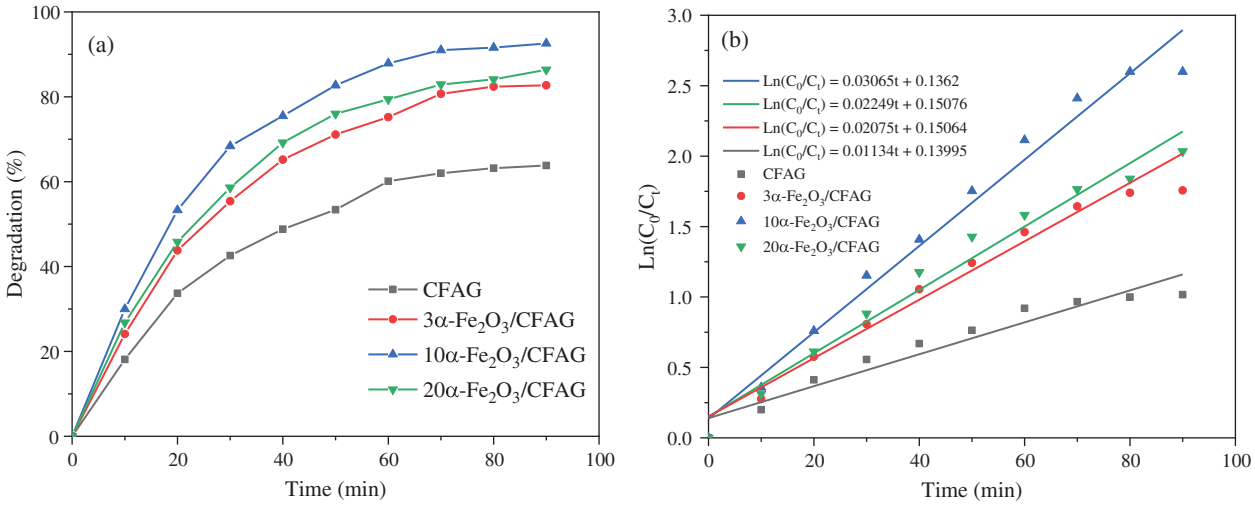

Figure 4: Degradation efficiency of (a) indigo carmine dye on various anodes, and the corresponding kinetic curves of (b) first order reaction

Table 3: Parameters of various kinetic models

Kinetic model	k (min^{-1})	R^2
Pseudo zero-order kinetic model	–0.13867	0.812
Pseudo first-order kinetic model	0.03065	0.979
Pseudo second-order kinetic model	0.01044	0.946

Fig. 5 shows the UV-vis absorption spectra of indigo carmine dye before and after electrocatalytic degradation over 10α-Fe_2O_3/CFAG composite anode. The spectrum of indigo carmine dye presents three main characteristic absorption peaks at the wavelengths of 250 nm, 285 nm, and 610 nm, and the

molecular structure of indigo carmine is inset in Fig. 5. The absorption peaks at 285 nm and 610 nm are related to the cross-conjugated system or chromophore of C=C and C=O in indigo carmine molecule, while the peak at 250 nm is assigned as the absorption of benzene ring structure [30,31]. After electrocatalytic degradation reaction, the peaks at 285 nm and 610 nm almost disappear, indicating that the cross-conjugated systems of chromophore are broken down and the chromaticity is removed. The peak still exists at 250 nm, but the intensity is obviously reduced, demonstrating that there may be a few intermediate products in the dye residue after the reaction.

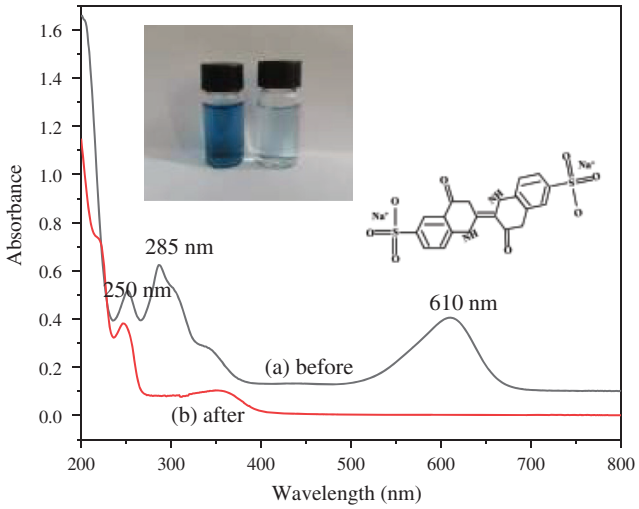

Figure 5: UV-vis spectra of indigo carmine dye before and after electrocatalytic degradation over 10α-Fe_2O_3/CFAG composite anode

3.4 Stability of as-Prepared Composite Anodes

The recycle stability of anode materials is an important parameter, reflecting whether it can be industrialized production, which has a great impact on the degradation efficiency and cost of wastewater treatment [13]. Fig. 6 shows the recycle stability assessment of 10α-Fe_2O_3/CFAG composite anode through five cycles. The degradation efficiency of indigo carmine dye decreases by 9.1% from initial 92.6% to 83.5% after five cycles, indicating that the α-Fe_2O_3/CFAG composite anode still has high electrocatalytic activity and favorable recycle stability in Fig. 6a. The catalytic effect reduced slightly after the cycling, which may be related to the reduction of surface active sites caused by the adsorption of organic molecules on the anode surface. Moreover, the XRD patterns of the 10α-Fe_2O_3/CFAG composite anode before and after electrpcatalytic degradations are almost same, implying that the composite anode remains good stability as shown in Fig. 6b.

3.5 Trapping Experiment of Hydroxyl Radical

To detect the active species in electrocatalytic process of indigo carmine dye degradation, the tertiary butyl alcohol (TBA) is selected as hydroxyl radical trapping agent. As shown in Fig. 7, the degradation efficiency of indigo carmine over 10-Fe_2O_3/CFAG reaches up 92.6% in the absence of free radical trapping agent. However, the degradation efficiency of indigo carmine decreases to 59.4% after the adding of TBA to the system for 90 min, indicating that hydroxyl radical has a significant influence on indigo carmine degradation in the electrocatalytic process. The formation of adsorbed hydroxyl radical MO_x(·OH) by oxidation of the water molecules has been reported as the initial reaction of MO_x anodes [32,33]. It can be described as follows:

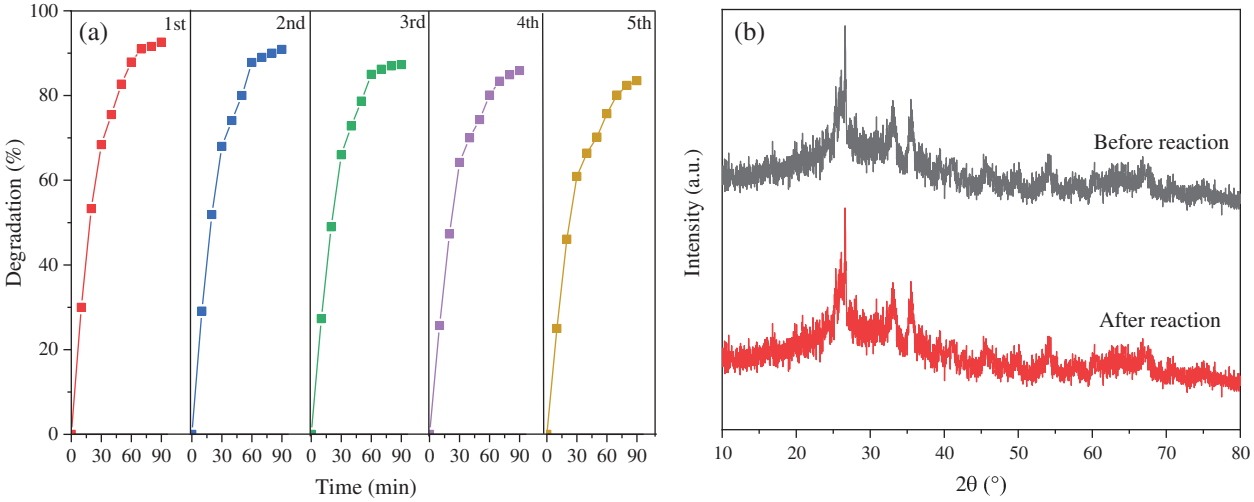

Figure 6: Stability of 10α-Fe_2O_3/CFAG composite anode of (a) cycle times, and (b) XRD patterns before and after degradation of indigo carmine dye

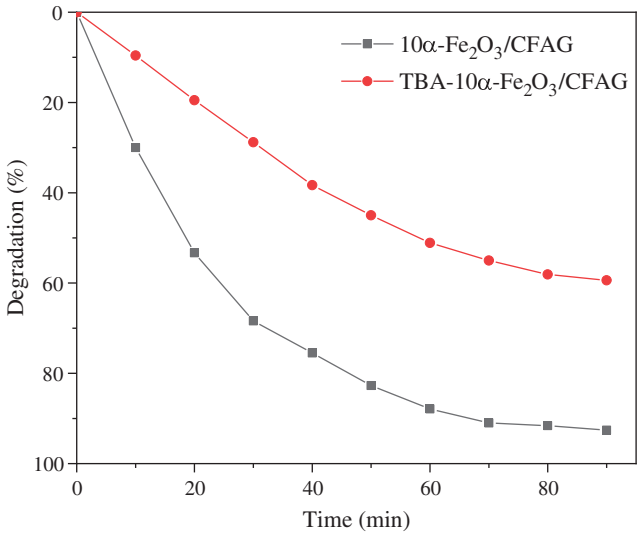

Figure 7: Trapping experiment of hydroxyl radical in electrocatalytic degradation of indigo carmine dye over 10α-Fe_2O_3/CFAG composite anode

$$MO_x + H_2O \rightarrow MO_x(\cdot OH) + H^+ + e^- \quad (2)$$

Then, the organic pollutants are degraded by electrochemically generated $MO_x(\cdot OH)$ with strong oxidative property. The main reaction was as follows:

$$R + MO_x(\cdot OH) \rightarrow MO_x + CO_2 + H^+ + e^- \quad (3)$$

In addition, under the action of electrocatalytic oxidation, the reaction can occur in anode as follows:

$$H_2O - 2e^- \rightarrow 2 \cdot OH + 2H^+ \quad (4)$$

Furthermore, the $MO_x(\cdot OH)$ can generate the O_2 gas, and this reaction acts as a competitor in the electrocatalytic degradation process as follows:

$$2MO_x(\cdot OH) \rightarrow 2MO_x + O_2 + 2H^+ + 2e^- \quad (5)$$

The addition of appropriate amount of α-Fe_2O_3 can decrease the interfacial resistance and increase oxygen evolution potential of the composite anode, thus inhibiting the side reaction and making more hydroxyl radicals act on organic pollutants.

4 Conclusions

In summary, a low-cost and high-efficiency α-Fe_2O_3/CFAG composite anode was successfully prepared via a facile dip-coating method and applied for dye wastewater treatment. The results demonstrated that the electrochemical performance of the α-Fe_2O_3/CFAG composite anode was closely related to the loading amount of α-Fe_2O_3. The α-Fe_2O_3 distributed on the surface of CFAG matrix with amorphous form under a low loading amount, while superabundant α-Fe_2O_3 aggregated resulting in the reduction of active sites. The α-Fe_2O_3/CFAG composite anode showed low oxygen evolution potential, great electrochemical active area, and small electrochemical impedance. In addition, the degradation rate of indigo carmine dye over the 10α-Fe_2O_3/CFAG composite anode approached to 92.6%, due to the generation of hydroxyl radical active species in the degradation process. The composite anode was long term active and reusable. Therefore, the synthesized α-Fe_2O_3/CFAG composite anode utilizing circulating fluidized bed fly ash not only enriched the types of electrocatalytic anode materials, but also had potential applications in treatment of dye wastewater.

Acknowledgement: This study was supported by the National Natural Science Foundation of China (No. 21676209), Key Research Development Project of Shaanxi Province (No. 2019GY-137) and the Cultivating Fund of Excellent Doctorate Thesis of Xi'an University of Architecture and Technology (No. 6040318008).

Funding Statement: The authors received no specific funding for this study.

Conflicts of Interest: The authors declare that they have no conflicts of interest to report regarding the present study.

References

1. Xue, F. F., Tang, B., Bin, L. Y., Ye, J. W., Huang, S. S. et al. (2019). Residual micro organic pollutants and their biotoxicity of the effluent from the typical textile wastewater treatment plants at Pearl River Delta. *Science of The Total Environment, 657,* 696–703. DOI 10.1016/j.scitotenv.2018.12.008.
2. Chen, S. X., Zhou, L. H., Yang, T. T., He, Q. H., Zhou, P. C. et al. (2020). Thermal decomposition based fabrication of dimensionally stable Ti/SnO_2-RuO_2 anode for highly efficient electrocatalytic degradation of alizarin cyanin green. *Chemosphere, 261,* 128201. DOI 10.1016/j.chemosphere.2020.128201.
3. Chowdhury, M. F., Khandaker, S., Sarker, F., Islam, A., Rahman, M. T. et al. (2020). Current treatment technologies and mechanisms for removal of indigo carmine dyes from wastewater: A review. *Journal of Molecular Liquids, 318,* 114061. DOI 10.1016/j.molliq.2020.114061.
4. Lei, J. N., Xu, Z. C., Xu, H., Qian, D., Liao, Z. W. et al. (2020). Pulsed electrochemical oxidation of acid Red G and crystal violet by PbO_2 anode. *Journal of Environmental Chemical Engineering, 8(3),* 103780. DOI 10.1016/j.jece.2020.103780.
5. Gong, Y. G., Wan, J. F., Zhou, P., Wang, X. R., Chen, J. et al. (2021). Oxygen and nitrogen-enriched hierarchical MoS_2 nanospheres decorated cornstalk-derived activated carbon for electrocatalytic degradation and supercapacitors. *Materials Science in Semiconductor Processing, 123(1–2),* 105533. DOI 10.1016/j.mssp.2020.105533.

6. Massa, A., Hernandez, S., Lamberti, A., Galletti, C., Russo, N. et al. (2017). Electro-oxidation of phenol over electrodeposited MnO_x nanostructures and the role of a TiO_2 nanotubes interlayer. *Applied Catalysis B: Environmental, 203,* 270–281. DOI 10.1016/j.apcatb.2016.10.025.
7. Brillas, E., Martinez-Huitle, C. A. (2015). Decontamination of wastewaters containing synthetic organic dyes by electrochemical methods. An updated review. *Applied Catalysis B: Environmental, 166,* 603–643. DOI 10.1016/j.apcatb.2014.11.016.
8. Zhou, Y. Z., Li, Z. L., Hao, C. T., Zhang, Y. C., Chai, S. N. et al. (2020). Electrocatalysis enhancement of α, β-PbO_2 nanocrystals induced via rare earth Er (III) doping strategy: Principle, degradation application and electrocatalytic mechanism. *Electrochimica Acta, 333,* 135535. DOI 10.1016/j.electacta.2019.135535.
9. Ansari, A., Nematollahi, D. (2020). Convergent paired electrocatalytic degradation of p-dinitrobenzene by Ti/SnO_2-Sb/β-PbO_2 anode. A new insight into the electrochemical degradation mechanism. *Applied Catalysis B: Environmental, 261,* 118226. DOI 10.1016/j.apcatb.2019.118226.
10. de Oliveira, G. R., Fernandes, N. S., de Melo, J. V., da Silva, D. R., Urgeghe, C. et al. (2011). Electrocatalytic properties of Ti-supported Pt for decolorizing and removing dye from synthetic textile wastewaters. *Chemical Engineering Journal, 168(1),* 208–214. DOI 10.1016/j.cej.2010.12.070.
11. Alcocer, S., Picos, A., Uribe, A. R., Perez, T., Peralta-Hernandez, J. M. (2018). Comparative study for degradation of industrial dyes by electrochemical advanced oxidation processes with BDD anode in a laboratory stirred tank reactor. *Chemosphere, 205(728),* 682–689. DOI 10.1016/j.chemosphere.2018.04.155.
12. Kong, Y., Wang, Z. L., Wang, Y., Yuan, J., Chen, Z. D. (2011). Degradation of methyl orange in artificial wastewater through electrochemical oxidation using exfoliated graphite electrode. *New Carbon Materials, 26(6),* 459–464. DOI 10.1016/S1872-5805(11)60092-9.
13. Chen, S. X., Li, J., Liu, L. Y., He, Q. H., Zhou, L. H. et al. (2020). Fabrication of Co/Pr Co-doped Ti/PbO_2 anode for efficiently electrocatalytic degradation of β-naphthoxyacetic acid. *Chemosphere, 256(2020),* 127139. DOI 10.1016/j.chemosphere.2020.127139.
14. Zhang, Y., He, P., Jia, L. P., Zhang, T. H., Liu, H. H. et al. (2019). Dimensionally stable Ti/SnO_2-RuO_2 composite electrode based highly efficient electrocatalytic degradation of industrial gallic acid effluent. *Chemosphere, 224,* 707–715. DOI 10.1016/j.chemosphere.2019.02.195.
15. Wu, J., Xu, H., Yan, W. (2015). Fabrication and characterization of β-PbO_2/α-PbO_2/Sb-SnO_2/TiO_2 nanotube array electrode and its application in electrochemical degradation of Acid Red G. *RSC Advances, 5(25),* 19284–19293. DOI 10.1039/C4RA16613B.
16. Xu, L., Li, M., Xu, W. (2015). Preparation and characterization of Ti/SnO_2-Sb electrode with copper nanorods for AR 73 removal. *Electrochimica Acta, 166,* 64–72. DOI 10.1016/j.electacta.2015.02.233.
17. Zhang, Y. J., Han, Z. C., He, P. Y., Chen, H. (2020). Geopolymer-based catalysts for cost-effective environmental governance: A review based on source control and end-of-pipe treatment. *Journal of Cleaner Production, 263(4),* 121556. DOI 10.1016/j.jclepro.2020.121556.
18. Asim, N., Alghoul, M. A., Mohammad, M., Amin, M. H., Akhtaruzzaman, M. et al. (2019). Emerging sustainable solutions for depollution: Geopolymers. *Construction and Building Materials, 199,* 540–548. DOI 10.1016/j.conbuildmat.2018.12.043.
19. Zhang, Y. J., Liu, L. C. (2013). Fly ash-based geopolymer as a novel photocatalyst for degradation of dye from wastewater. *Particuology, 11(3),* 353–358. DOI 10.1016/j.partic.2012.10.007.
20. El-Said, W. A., AlMalki, M. A., Sayed, E. M., El-Hady, D. A., Alshitari, W. (2020). Development of copper oxide nanostructures modified indium tin oxide electrode for electrochemical catalytically oxidation of methanol. *Materials Letters, 279(5),* 128498. DOI 10.1016/j.matlet.2020.128498.
21. Choi, S. C., Lee, W. K. (2012). Effect of Fe_2O_3 on the physical property of geopolymer paste. *Advanced Materials Research, 586,* 126–129. DOI 10.4028/www.scientific.net/AMR.586.126.
22. Chen, F., Wang, K. T., Shao, L., Muhammad, Y., Wei, Y. Z. et al. (2019). Synthesis of Fe_2O_3-modified porous geopolymer microspheres for highly selective adsorption and solidification of F^- from waste-water. *Composites Part B: Engineering, 178,* 107497. DOI 10.1016/j.compositesb.2019.107497.

23. He, P. Y., Zhang, Y. J., Chen, H., Han, Z. C., Liu, L. C. (2019). Low-energy synthesis of kaliophilite catalyst from circulating fluidized bed fly ash for biodiesel production. *Fuel, 257(3),* 116041. DOI 10.1016/j.fuel.2019.116041.
24. Harraz, F. A., Faisal, M., Jalalah, M., Almadiy, A. A., Al-Sayari, S. A. et al. (2020). Conducting polythiophene/ α-Fe_2O_3 nanocomposite for efficient methanol electrochemical sensor. *Applied Surface Science, 508(38),* 145226. DOI 10.1016/j.apsusc.2019.145226.
25. Yu, S., Hao, C. T., Li, Z. L., Zhang, R. R., Dang, Y. et al. (2021). Promoting the electrocatalytic performance of PbO_2 nanocrystals via incorporation of Y_2O_3 nanoparticles: Degradation application and electrocatalytic mechanism. *Electrochimica Acta, 369,* 137671. DOI 10.1016/j.electacta.2020.137671.
26. Zhang, Y., He, P., Jia, L. P., Li, C. X., Liu, H. H. et al. (2019). Ti/PbO_2-Sm_2O_3 composite based electrode for highly efficient electrocatalytic degradation of alizarin yellow R. *Journal of Colloid and Interface Science, 533,* 750–761. DOI 10.1016/j.jcis.2018.09.003.
27. Urbanczyk, E., Maciej, A., Simka, W. (2020). Electrocatalytic properties of Co decorated graphene and graphene oxide for small organic molecules oxidation. *International Journal of Hydrogen Energy, 45(3),* 1769–1783. DOI 10.1016/j.ijhydene.2019.11.036.
28. Zhou, Y. Z., Zhang, Y. C., Li, Z. L., Hao, C. T., Wang, Y. et al. (2020). Oxygen reduction reaction electrocatalysis inducing Fenton-like processes with enhanced electrocatalytic performance based on mesoporous ZnO/CuO cathodes: Treatment of organic wastewater and catalytic principle. *Chemosphere, 259,* 127463. DOI 10.1016/j.chemosphere.2020.127463.
29. Liu, Y., Liao, H. B., Zhou, Y., Du, Y. H., Wei, C. et al. (2015). Fe_2O_3 nanoparticle/SWCNT composite electrode for sensitive electrocatalytic oxidation of hydroquinone. *Electrochimica Acta, 180,* 1059–1067. DOI 10.1016/j.electacta.2015.09.046.
30. Vautier, M., Guillard, C., Herrmann, J. M. (2001). Photocatalytic degradation of dyes in water: Case study of indigo and of indigo carmine. *Journal of Catalysis, 201(1),* 46–59. DOI 10.1006/jcat.2001.3232.
31. Zhang, Y. J., He, P. Y., Zhang, Y. X., Chen, H. (2018). A novel electroconductive graphene/fly ash-based geopolymer composite and its photocatalytic performance. *Chemical Engineering Journal, 334,* 2459–2466. DOI 10.1016/j.cej.2017.11.171.
32. Comninellis, C. (1994). Electrocatalysis in the electrochemical conversion/combustion of organic pollutants for waste water treatment. *Electrochimica Acta, 39(11–12),* 1857–1862. DOI 10.1016/0013-4686(94)85175-1.
33. Dargahi, A., Ansari, A., Nematollahi, D., Asgari, G., Shokoohi, R. et al. (2019). Parameter optimization and degradation mechanism for electrocatalytic degradation of 2, 4-diclorophenoxyacetic acid (2, 4-D) herbicide by lead dioxide electrodes. *RSC Advances, 9(9),* 5064–5075. DOI 10.1039/C8RA10105A.